Mixed Convection from Tandem Semi-Circular Cylinders Arranged in a Vertical Channel

Gupta, Rakesh K., Chandra, Avinash*+; Gupta, Raj K.

Department of Chemical Engineering, Thapar Institute of Engineering & Technology, Patiala, Punjab, INDIA

ABSTRACT: *Semi-circular cylinders provide better space economy than circular and other non-circular cylinders. The cylinders are frequently used in a tandem arrangement in heat transfer equipment. The present study aims to obtain the flow and heat transfer characteristics for the tandem arrangement of semi-circular cylinders. The cylinders are placed in a vertical channel with a blockage (β) of 0.2. The upward flow under the reverse gravity is considered here. The influence of various parameters such as Reynolds number (Re), Prandtl number (Pr), Richardson number (Ri), and spacing between cylinders (YC) is observed. The governing parameters are varied in a range of 1 ≤ YC ≤ 6, 1 ≤ Re ≤ 50, 0.7 ≤ Pr ≤ 50, and 0 ≤ Ri ≤ 2. The numerical results are obtained by solving governing equations using FVM (Finite volume method). The velocity field, thermal field, drag coefficient (CD), pressure coefficient (Cp), and average Nusselt number (Nuavg) are presented. The increase in Re and Pr has enhanced the Nuavg and CD, whereas Ri and YC have shown complex dependency. The obtained results show that the mutual interaction of upstream and downstream cylinders has vanished for YC > 4. The upstream and downstream cylinders have shown different behavior at identical operating conditions. The drag coefficient for the upstream cylinder varies with YC for 1 ≤ Re ≤ 10, whereas for 10 ≤ Re ≤ 50, it shows negligible change except for the case of Pr = 0.7 and Ri = 2. The drag on the downstream cylinder increases monotonically with an increase in YC. The average Nusselt number for both cylinders increased with an increase in YC except for the downstream cylinder at Re = 1 and Pr = 0.7. Overall, the complex interplay of governing parameters has been observed in the flow and thermal characteristics.*

KEYWORDS: *Mixed convection; Semi-circular cylinder; Blockage ratio; Reynolds number; Richardson number; Nusselt number; Drag coefficient.*

INTRODUCTION

Heat transfer from cylinders of circular and non-circular cross-sections are closely related to the existing industrial processes and applications like different types of heat exchanging equipment, solar power systems, oil and gas distribution lines, cooling of various hardware system used in IT industries, thermal treatment of foodstuffs in continuous processing facilities, etc. [1,2]. The cylinders of the circular cross-section are very common in industry and household applications due to their simple construction and well-settled available technology for more than a hundred years. Due to recent technological developments, the cylinders of other cross-sections are

* *To whom correspondence should be addressed.*
+ *E-mail: avichiitk@gmail.com*
1021-9986/2023/6/1946-1961 16/$/5.06

Table 1: Comparison of values of Nu_{avg} and C_D of forced convection heat transfer from a cylinder of a particular cross-section to a Newtonian fluid.

S. No.	Cross-section of the cylinder	Operating conditions	Nu_{avg}	C_D	Reference
1	Circular	Re = 40, Pr = 50	14.0	1.4987	[24]
2	Equilateral triangular	Re = 50, Pr = 50	19.3	…	[25]
3	Semi-circular	Re = 40, Pr = 50	16.7	1.54	[26]
4	Square with its side at 45° to the incident flow	Re = 40, Pr = 50	15.4	0.51	[27]
5	Square with its side in line with incident flow	Re = 40, Pr = 50	12.6	0.95	[28]

also used for specific purposes and gaining popularity day by day. In this context, several research works were conducted over the years and explored the physics behind heat transfer from non-circular cylinders. These studies are needed to understand and improve our engineering applications, leading to new technology for specific applications. It will also help to deal with the space constraints and efficiency of the thermal systems.

The cylinders of non-circular cross-sections, like semi-circular, square, triangular, elliptical, etc., are also widely used in recent heat transfer applications. Solar water heating, novel heat transfer processes for electronic equipment cooling, chimney stacks, nuclear reactor cooling, cooling towers, building works, oil and gas pipelines, material processing, etc. [3-7] are examples of such applications. In the broad class of non-circular cylinders, the semi-circular cross-section has the natural benefit of occupying less space to deal with space economy compared to other non-circular and circular cross-sections. The comparison of the performance of cylinders of different types of cross-sections in forced convection heat transfer to Newtonian fluids is listed in Table 1. This table shows that semi-circular cylinders offer the highest value of Nu_{avg} and the lowest value of C_D. Hence, it can be regarded as one of the best options for heat transfer from cylinders to fluids. Several studies relating to applications of the semi-circular cylinder are found in various references listed here [2,8-23]. Most relevant and recent studies related to the present work from the available body of literature are summarized here. In one of the preliminary numerical simulation works, Chandra and Chhabra [11] explored the flow and thermal characteristics of a heated semi-circular cylinder without confinement to fluids of Newtonian nature in a range of $0.01 \leq Re \leq 40$ and $Pr \leq 100$. They reported the drag coefficients, recirculation length, Nusselt number, and critical Reynolds number for the range of governing parameters. In the continuation, they said the beginning of flow separation at Reynolds number of 0.575 and vortex shedding at Reynolds number of 39.75. These critical Reynolds number values were observed to be lesser than their counter values for circular and square cylinder cylinders. Heat transfer at the curved surface was found to be more than the value at the flat surface of the semi-circular cylinder.

Further, they [10] extended the work for power-law fluids also. They found a more intense impact of the power-law index at higher Prandtl numbers. The other orientation of the semi-circular cylinder, with a flat side parallel to the direction of fluid movement, was also presented by Gode et al. [2] for $0.01 \leq Re \leq 120$ and $1 \leq Pr \leq 50$ and reported flow to be steady up to $Re = 120$. Furthermore, Bhinder et al. [12] worked on momentum and thermal characteristics in the vicinity of a heated semi-circular cylinder at different angles (0-180 degrees) to the airflow at $80 \leq Re \leq 180$ and confirmed three types of separation zones according to incidence angle values. Another study by Chandra and Chhabra [13] shows heat transfer characteristics from unconfined heated semi-circular cylinders to fluids under mixed convection. They worked on Newtonian and power-law fluids at operating conditions of $1 \leq Re \leq 30$, $1 \leq Pr \leq 100$, and $0 \leq Ri \leq 2$. The maximum local Nusselt number was shifted from the corner to the front stagnation point when a value of Re went from 1 to higher values. The pressure coefficient value was also seen as a maximum at the front stagnation point at all times. The increase in the value of the Richardson number resulted in an increase in the drag coefficient and average Nusselt number.

Further, the effect of buoyancy perpendicular to flow direction on a semi-circular cylinder confined in a channel was numerically investigated by *Sukesan* and *Dhiman* [15] for $Re = 1–40$, $Ri = 0–4$, $Pr = 0.71–50$ and β (confinement ratio) as 0.1667–0.5. They have reported the drag coefficients and Nusselt numbers as dependent on Ri or β. They observed an increment in the drag coefficients and Nusselt number due to a rise in Ri and β values at every Reynolds number other than 1 in case of an increase in Nu.

In our previous work, a numerical study on the semi-circular cylinder was done for heat transfer under buoyancy [20] for the operating parameters as $0.2 \leq \beta \leq 0.8$, $1 \leq Re \leq 50$, $0.7 \leq Pr \leq 50$ and $0 \leq Ri \leq 2$. They observed a steady flow for a complete range of Reynolds numbers. The maximum pressure coefficient and C_D value increased with a rise in β value for the channel. The values of C_D and Nu_{avg} (at all conditions except $Re = 1$) also exhibited to increase with the buoyancy of the flow.

Furthermore, multiple cylinder arrangements can be seen in industrial/practical engineering applications like solar water heaters, cooling of a nuclear reactor, cooling of electronic equipment, etc. Multiple cylinder arrangements are classified as tandem/in-line, side by side, and staggered. In this context, the available literature is summarized in the following text. Few researchers [29] experimentally investigated heat transfer from cylinders to air under gravity for an operating range of $0.01 \leq Re_f \leq 45$ and temperature difference in a range of more than 30 °C and proposed different correlations. Another group of researchers [30] conducted simulation work for circular cylinders in tandem orientation on buoyancy added heat transfer at a distance (Y_C) of 1.5-7 in adiabatic confined walls at $\beta = 0.1$-0.67, $Re = 40$, $Pr = 0.7$ and $Ri = 0.1$-10. It was observed that the overall heat transfer coefficient was increased at larger cylinder spacing at $\beta < 0.33$. Moreover, the value of Nu_{avg} of the upstream cylinder was reported independent of the distance between cylinders, although the value of Nu_{avg} of downstream one showed dependency on cylinder spacing. At $Ri \leq 1$, the value of Nu_{avg} of the upstream cylinder was seen as higher compared to the downstream one. Further, in another study [31], numerical mixed convection heat transfer was also investigated from cylinders in tandem between vertical plates for cylinder spacing (Y_C) as 1.5. Simulations were carried out for operating parameters as $\beta = 0.4$-0.67, $Re = 50$-100, $Pr = 0.7$ and $-5 \leq Ri \leq 5$. For $\beta = 0.4$ and $Re = 50$, the Nu_{avg} value was reported to increase with a rise in the value of Ri.

Chatterjee [1] numerically studied heat transfer for cylinders of the square cross-section in tandem arrangement and placed with a distance of four widths of the cylinder in a channel for β value as 0.25 under gravity effect. The study was conducted with the vertical flow of air ($Pr = 0.7$) at $1 \leq Re \leq 30$ and $-1 \leq Ri \leq 1$. They observed that, for a higher value of Re, the size of recirculation zones behind cylinders was reported to decrease with an increase in Ri. Heat transfer from cylinders increased with an increase in the buoyancy effect. Higher heat transfer was also observed for the downstream cylinder than for the upstream one. These effects may be because of the combined shape of the cylinder and operating parameters.

Mixed convection heat transfers from semi-circular cylinders in different arrangements have also been studied by different investigators. The semi-circular (inclined) with a square cylinder in the tandem arrangement was studied by *Sisodia et al.* [19], and flow as well as thermal characteristics were presented for $Pr = 0.71$, $10 < Re < 45$, $0 \leq \alpha$ (incidence angles) $\leq 180°$ and $0 \leq Ri \leq 2$ in crossflow. The joint influences of thermal buoyancy with the angle of incidence were explored, and they reported the critical values as $Re > 40$, $Ri = 0.5$ at $\alpha = 30°$ and $Re \leq 20$ at $\alpha = 90°$, $Ri = 0.5$ for the onset of vortex shedding. They found a minimum value of Nu_{avg} when the flat side of the semi-circular cylinder was oriented parallel to the flow direction. Buoyancy-aided heat transfer [32] was studied from semi-circular cylinders in the tandem arrangement between vertical confinement for $\beta = 0.2$, $Y_C = 3$, $Re = 200$, $Pr = 0.7$ and $-1 \leq Ri \leq 1$. They reported an influence of the upstream cylinder on the downstream with lower heat transfer from the later one. Both cylinders showed the value of Nu_{avg} as higher for buoyancy-assisted cases. In another study by Parthasarathy et al. (2017), the optimum number of semi-circular cylinders on a side-by-side arrangement and the optimum gap between the cylinders were studied for $Re = 100$ with air. They reported no significant interaction in the flow for space between cylinders greater than four times diameter and concluded good heat transfer downstream of the cylinders at a lower gap. Furthermore, some studies are also available on the flow and heat transfer from porous bluff bodies for potential application in developing heat transfer devices for electronic cooling, solar heating, etc. [33-35].

The above literature review shows that the bank of semi-circular cylinders has a scope for the development of efficient and compact heat transfer technology. This literature review also reveals that the present study about the semi-circular cylinder in tandem arrangements under channel confinement is missing in the available body of literature. It is important in sophisticated cooling applications such as efficiently cooling electronic components under confined spaces. The recent developments in the electronic industry involve the miniaturization of electronic components and gadgets with high efficiency. The increased efficiency

produces excess

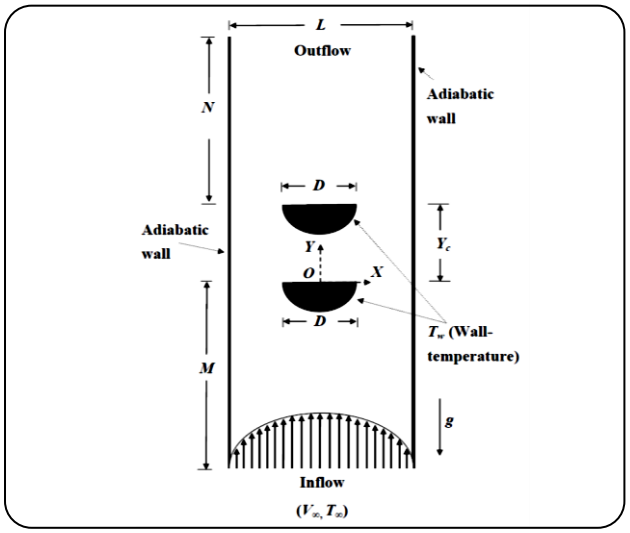

Fig. 1: Schematic of mixed convection heat transfer from tandem semi-circular cylinders arranged in a vertical channel.

heat due to higher current flow in the components. This extra heat is required to be removed for the safety of the devices. Moreover, these electronic devices can also malfunction at higher temperatures. Hence, an effective and efficient heat removal mechanism is necessary for a geometrically similar system like the present case study for semi-circular cylinders in confinement.

Additionally, the proposed configuration can be idealized for several industrial situations, such as heat exchangers in food processing, polymer processing, nuclear reactors, etc. Moreover, mixed convection has become important for improving heat rejection in electronic sources without confinement and in enclosures [36,37]. The combined effect of forced and natural convection has gained popularity in examples involving atmospheric flows, drying technologies, etc. [38]. Various nanofluids are also used to enhance heat rejection; sometimes, they may also be coupled with magnetohydrodynamics convection [7,37,39,40].

Therefore, the present study aims to explore flow and thermal characteristics around a pair of heated semi-circular cylinders in tandem under confinement (β = 0.2) to Newtonian fluids for the ranges of governing parameters as $1 \le Y_C \le 6$, $1 \le Re \le 50$, $0.7 \le Pr \le 50$ and $0 \le Ri \le 2$.

THEORETICAL SECTION

Problem statement

Here, 2D simulations are executed to explore the flow and thermal characteristics around semi-circular cylinders in tandem in the presence of the gravity effect. A pair of similar cylinders (each of diameters D) are placed in a vertical row between a rectangular channel of width L, as shown in Fig. 1. The curved surfaces of cylinders are faced downwards, and their centers are aligned at the centreline of the channel. The distance from the channel inlet to the center of the upstream cylinder is M, between the centres of cylinders is Y_C, and from the center of the downstream cylinder to the channel outlet is N. The fixed channel confinement (β) is taken as 0.2 in the present study.

Both cylinders are kept at a constant temperature of T_w, and channel walls are considered adiabatic. A Newtonian fluid at uniform velocity (V_∞) and temperature (T_∞) is allowed to flow in the channel vertically upwards against gravity. The convective flow is aided by buoyancy caused by the density decrease of the fluid due to heat transfer from the cylinders. Due to the slight temperature difference ($T_w - T_\infty$= 1) between fluid and cylinders, the thermal and physical fluid properties are considered fixed. Moreover, the variation of fluid densty is approximated by the Boussinesq equatio as $\rho = \rho_\infty[1 - \beta_V(T - T_\infty)]$. The contribution of viscous dissipation is neglected due to lower velocity gradients at the study's prevailing values of Reynolds number and Richardson number. The mass, momentum and energy equations are in-line with the literature [1,13,15,19,20].

Hence, the obtained governing Equations (1-4) are as follows in dimensionless form.

Mass equation: $$\frac{\partial u}{\partial x} + \frac{\partial v}{\partial y} = 0 \quad (1)$$

Momentum equations:

$$u\frac{\partial u}{\partial x} + v\frac{\partial u}{\partial y} = -\frac{\partial p}{\partial x} + \frac{1}{Re}\left(\frac{\partial^2 u}{\partial x^2} + \frac{\partial^2 u}{\partial y^2}\right) \quad (2)$$

$$u\frac{\partial v}{\partial x} + v\frac{\partial v}{\partial y} = -\frac{\partial p}{\partial y} + \frac{1}{Re}\left(\frac{\partial^2 v}{\partial x^2} + \frac{\partial^2 v}{\partial y^2}\right) + Ri.\theta \quad (3)$$

Energy equation:

$$u\frac{\partial \theta}{\partial x} + v\frac{\partial \theta}{\partial y} = \frac{1}{Re.Pr}\left(\frac{\partial^2 \theta}{\partial x^2} + \frac{\partial^2 \theta}{\partial y^2}\right) \quad (4)$$

where the dimensionless parameters are defined as $x = X/D$, $y = Y/D$, $u = U/V_\infty$, $v = V/V_\infty$, $p = P/\rho V_\infty^2$, $\theta = [T - T_\infty]/[T_w - T_\infty]$, $Re = DV_\infty\rho/\mu$, $Ri = g\beta_V(T - T_\infty)D/V_\infty^2$

These equations (1-4) are bound by the conditions given below:

Channel entrance: $u = 0$, $v = 1.5(1 - 2\beta|x|)^2$ where $\beta = 0.2$ [20] and $\theta = 0$

At the channel entrance, the inlet parabolic velocity

Table 2: Results of validation work.

	Chandra and Chhabra [13]	Farouk and Guceri [41]
Operating parameters	Re = 20, Pr = 0.7	Re = 58.01, Pr = 0.7, Ri = 4.12
Literature values	C_{DP} = 1.313 [13] C_D = 1.993 [13] Nu_{avg} = 3.64 [13]	Nu_{avg} = 6.63 [41]
Present values	C_{DP} = 1.315 C_D = 1.995 Nu_{avg} = 3.52	Nu_{avg} = 6.40

profile is considered, as shown in the above equation. To tackle the entrance effect, a sufficiently sizeable computational inlet domain has been used for each case. It is already known that the large inlet domain can vanish the inlet disturbances, and the change in the velocity gradients is stabilized before approaching the first cylinder.

Channel walls: $u = 0$, $v = 0$ and $\partial\theta/\partial x = 0$

Cylinder surface: $u = 0$, $v = 0$ and $\theta = 0$

Centreline of the channel ($x = 0$): Laminar flow, $u = 0$, $\partial v/\partial x = 0$ and $\partial\theta/\partial x = 0$

Channel exit: Fully developed flow, $\partial\varphi/\partial y = 0$, where $\varphi = u$, v and θ

The solutions of the above governing equations (1-4) are calculated and reported in terms of different flow and thermal variables as u, v, p, and θ. Further, these variables are used to calculate parameters such as total drag coefficient, pressure coefficient, local Nusselt number and average Nusselt number. The values of the above essential parameters are defined in equations 5-8.

$$C_D = \frac{F_D}{\frac{1}{2}\rho {v_\infty}^2 D} \quad (5)$$

$$C_P = \frac{P_S - P_\infty}{\frac{1}{2}\rho {v_\infty}^2} \quad (6)$$

$$Nu = -\frac{\delta\theta}{\delta n_S} \quad (7)$$

$$Nu_{avg} = \frac{1}{S}\int_S Nu.dS \quad (8)$$

Numerical Methodology

A two-dimensional mesh model of the present problem is prepared in the Gambit pre-processor. Combinations of triangular and quadrilateral meshes are used to prepare an equivalent mesh model. Fine meshes are used near the cylinders to capture the high gradients of different property values, and coarser meshes are used away from cylinders. More than 99.99% of meshes have skewness as low as in a range of 0-0.4, and the value of maximum skewness of the rest of the meshes is found as 0.605. Further, a two-dimensional, steady, and pressure-based solver of the Ansys Fluent is used to solve governing equations (1-4), in particular, the operating conditions of the problem. A laminar viscous model is used to depict the flow behavior in the study. The momentum and energy equations have been solved using a second-order upwind scheme where the SIMPLE (Semi Implicit Methods for Pressure Linked Equations) technique is adopted for pressure velocity coupling. The numerical tolerance limits for the residuals for continuity and momentum equations (1-3) are set down as 10^{-8} and 10^{-15} for energy equation (4). The above details of numerical solutions are in-line with our previous work [20].

To ensure the reliability of the solution technique with the choice of numerical parameters to be used in simulation experiments, previous studies [13,41] have been selected to validate our numerical methodology. The comparison of reproduced results with literature values is presented in table 2. The reproduced results for selected studies show that the results are accurate within ±3.5%. The extended details of validation works are given in our previous work [20]. Therefore, the proposed methodology is adequate to study mixed convection heat transfer from confined semi-circular cylinders.

RESULTS AND DISCUSSION

Domain and Grid Independence

Before moving further, it is always good to choose a suitable domain size and mesh size for simulation problems to optimize time and computational resources. Optimized domain and mesh provide accurate solutions, independent of their size. Initially, inlet domain independence test is conducted at m = 30, 40 and 50, n = 60 for extreme values of operating parameters as $Y_C = D$ & $6D$, Re = 1 & 50, Pr = 0.7 & 50 and Ri = 0 & 2. Simulated values of C_{D1}, C_{D2}, Nu_{avg1} and Nu_{avg2}, at different values of m, are obtained and presented in Table 3. For m = 40 and 50 (Table 3), the changes in C_{D1}, C_{D2}, Nu_{avg1} and Nu_{avg2} are observed to be a maximum of 1.1%.

Table 3: Results of inlet domain independence tests.

Y_C	m	n	Re	Pr	Ri	C_{D1}	C_{D2}	Nu_{avg1}	Nu_{avg2}
1	30	60	1	0.7	0	17.91	14.18	0.7464	0.3345
	40					17.84	14.15	0.7463	0.3346
	50					17.84	14.16	0.7463	0.3346
	30		50	50	2	2.05	0.810	20.55	7.160
	40					2.09	0.804	20.88	7.050
	50					2.11	0.800	20.97	7.030
6	30		1	0.7	0	22.32	22.32	0.915	0.3006
	40					22.31	22.33	0.915	0.3006
	50					22.31	22.33	0.915	0.3006
	30		50	50	2	2.170	1.926	20.90	16.67
	40					2.210	1.936	21.10	16.66
	50					2.240	1.941	21.20	16.64

Table 4: Results of outlet domain independence tests.

Y_C	m	n	Re	Pr	Ri	C_{D1}	C_{D2}	Nu_{avg1}	Nu_{avg2}
1	40	50	1	0.7	0	17.84	14.15	0.7463	0.3346
		60				17.84	14.15	0.7463	0.3346
		50	50	50	2	2.092	0.8042	20.88	7.049
		60				2.092	0.8042	20.88	7.049
6	40	50	1	0.7	0	22.32	22.33	0.9153	0.3006
		60				22.32	22.33	0.9153	0.3006
		50	50	50	2	2.213	1.936	21.10	16.66
		60				2.213	1.936	21.10	16.66

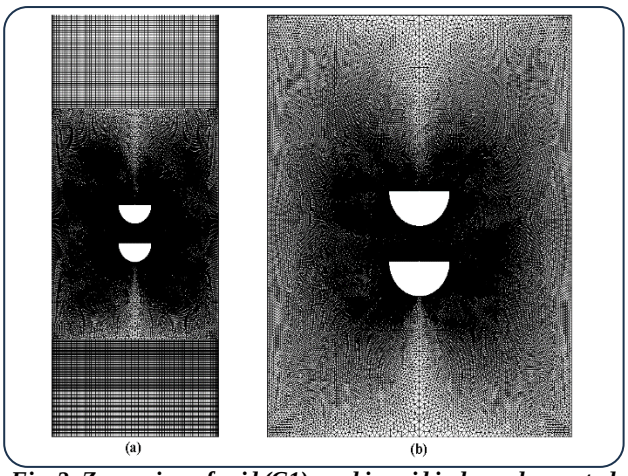

Fig. 2: Zoom view of grid (G1) used in grid independence study for Y_C = 1.

Therefore, m = 40 has been chosen as the optimized value of inlet domain size for the present work. Then, outlet domain independence test is conducted for value of n = 50 & 60 and other parameters as m = 40, Y_C = D & 6D, Re = 1 & 50, Pr = 0.7 & 50 and Ri = 0 & 2. The values of C_{D1}, C_{D2}, Nu_{avg1} and Nu_{avg2}, at both values of n, are obtained and reported in Table 4. For n = 50 and 60 (Table 4), the maximum change in the values of C_{D1}, C_{D2}, Nu_{avg1} and Nu_{avg2} is observed as 0.002%. Therefore, n = 50 has been selected as the optimized value of outlet domain size. Further, two different grids (G1 and G2) are used to run the grid independence tests with an optimized domain for extreme operating conditions [20]. The results of these simulations are reported in Table 5, and the maximum change in C_{D1}, C_{D2}, Nu_{avg1} and Nu_{avg2} is observed as 0.49%. Therefore, optimized grid G1 is finalized for further simulations at all operating conditions of the study, as given in Fig. 2.

Flow characteristics

The flow characteristics are provided in this section in terms of streamline profiles, pressure variation and the drag coefficient for the chosen range of the governing parameters.

Streamline profiles

Fig. 3 shows streamline profiles at extreme values of Re, Pr and Ri for Y_C = 1, 3, 5 and 6. At Re = 1 and Y_C = 1, the streamlines follow the body shape and are attached to cylinders because of the domination of viscous forces at low Re. Further, a wake formation is seen in the space between the cylinders for the complete range of Pr and Ri. This wake formation is due to the obstruction created by the downstream cylinder to the upcoming flow. At Re = 1 and higher values of Y_C = 3, 5 and 6, the streamlines are again found attached to both the cylinders without wake formation at low Re. Specifically, for $Y_C \geq 3$, the streamlines of the first cylinder are reported to be unaffected by the second cylinder in all cases of Re = 1. It can be said here that the presence of the second (downstream) cylinder is not affecting the flow dynamics of the upstream cylinder. Moreover, this phenomenon is not changed during the increase of Pr and Ri values for every set of Y_C.

Furthermore, at a higher value of Re = 50, the wake formation behind the upstream cylinder has been observed at all Y_C, Pr and Ri values except for Pr = 50 and Ri = 2. It can be seen here that the wake size is decreasing with

Table 5: Results of grid independence tests.

Y_C	Re	Pr	Ri	Grid	δ	n_p	G_N	C_{D1}	C_{D2}	Nu_{avg1}	Nu_{avg2}
1	1	0.7	0	G1	0.007	184	132152	17.837	14.15	0.7463	0.3346
				G2	0.0048	268	226352	17.833	14.15	0.7464	0.3345
	50	50	2	G1	0.007	184	132152	2.0920	0.8042	20.88	7.05
				G2	0.0048	268	226352	2.0929	0.8045	20.83	7.04
6	1	0.7	0	G1	0.007	184	132152	22.316	22.33	0.9153	0.3006
				G2	0.0048	268	248138	22.312	22.33	0.9153	0.3006
	50	50	2	G1	0.007	184	177216	2.2129	1.936	21.10	16.66
				G2	0.0048	268	248138	2.2131	1.937	21.05	16.57

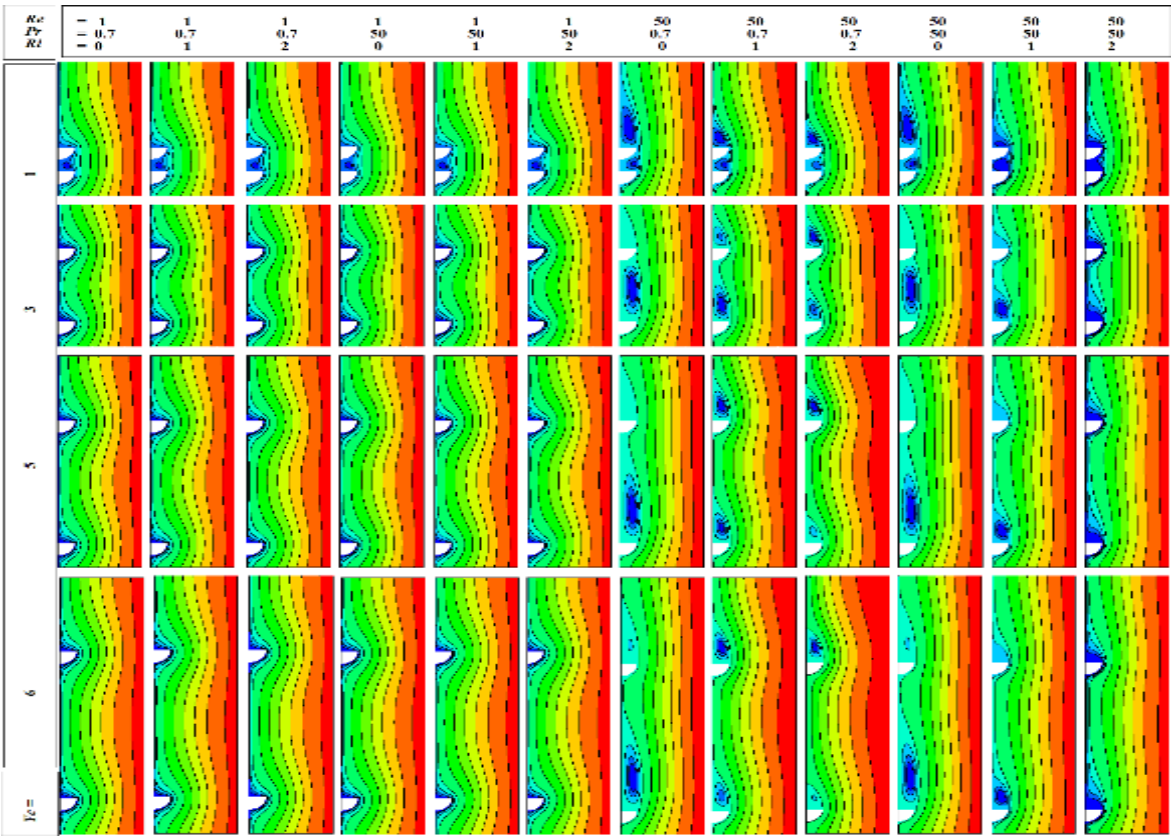

Fig. 3: Streamline profiles at different values of Y_C, Re, Pr and Ri.

The increasing value of *Ri*. As *Ri* increases, the influence of the gravity (body force) is increased in the opposite direction to the flow, leading to the wake vanishing at *Ri* = 2. At *Re* = 50 and *Ri* = 0, the wake size behind the upstream cylinder is found to increase, which is evident due to the increased influence of the inertial forces with rising *Re*. Again, the wake size increases with an increase in the space between the cylinders for $1 \leq Y_C \leq 5$. Further increment in Y_C value to 6, no change in wake size is observed due to the negligible influence of the downstream cylinder on the upstream one. At *Re* = 50 and *Ri* = 1, the wake size behind the upstream cylinder is found to increase for $1 \leq Y_C \leq 3$ and then to decrease for $5 \leq Y_C \leq 6$. At *Re* = 50, *Ri* = 2 and *Pr* = 0.7, wake size behind the upstream cylinder is also found to increase for $1 \leq Y_C \leq 3$ and then decrease for $5 \leq Y_C \leq 6$. Further, at *Re* = 50 and *Ri* = 0, the wake size behind the downstream cylinder decreases in size as the value of Y_C increases. At *Re* = 50, *Ri* = 1 and *Pr* = 0.7, wake size behind the downstream cylinder decreases at $1 \leqslant Y_C \leqslant 3$, later increasing and becoming constant in a range of $5 \leq Y_C \leq 6$. At *Re* = 50, *Ri* = 2 and *Pr* = 0.7, wake size behind downstream cylinder is found to increase for $1 \leq Y_C \leq 3$ and later has become constant in the range of $3 \leq Y_C \leq 6$. At *Re* = 50, *Pr* = 50 and *Ri* = 1, wake size behind the downstream

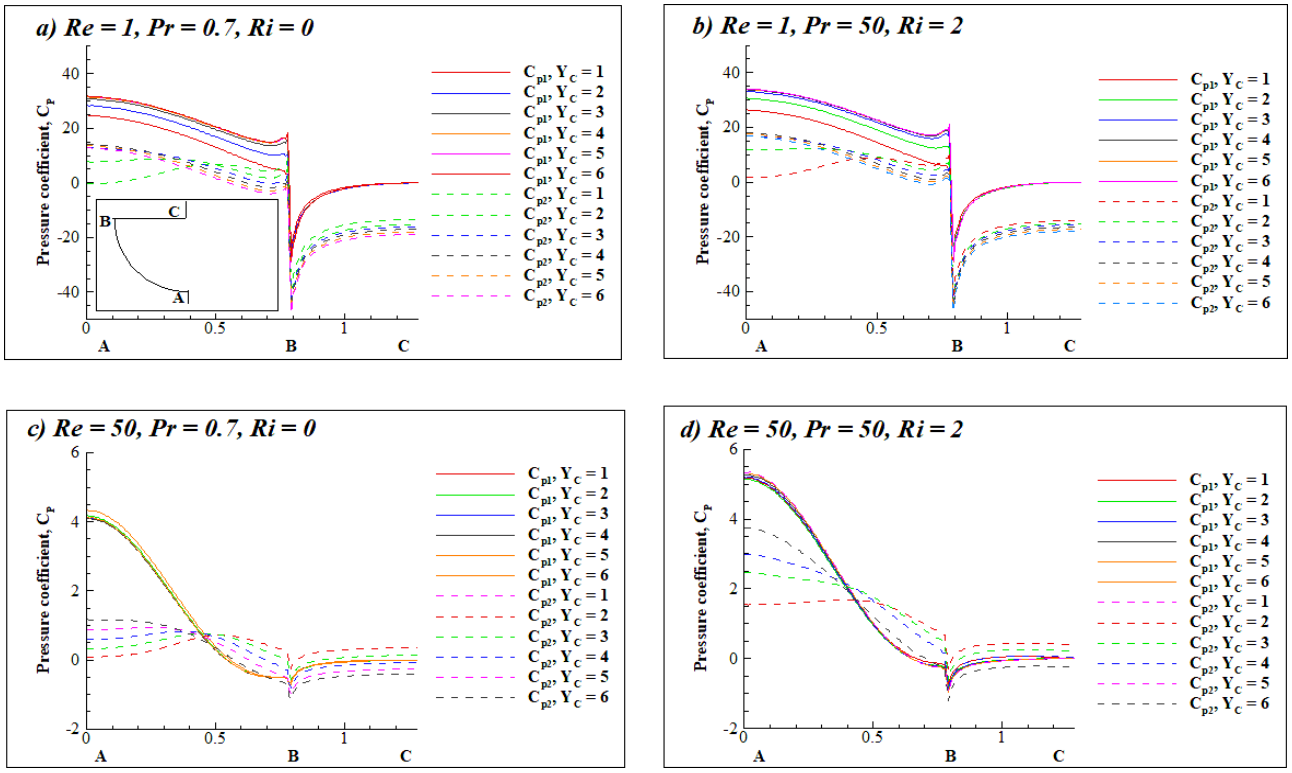

Fig. 4: Variation of pressure coefficients at cylinder surface for different values of Re, Pr, Ri and Y_C.

cylinder is observed to be constant with an increase in the value of Y_C. At Re = 50, Pr = 50, and Ri = 2, the wake behind the downstream cylinder has almost disappeared for all values of Y_C. These phenomena are the result of the complex influence of the governing parameters on the flow field. Therefore, the wake sizes behind both cylinders show complex dependence on Y_C and Ri.

Variation of pressure coefficients

Detailed flow behavior is explored with the values of pressure coefficients (C_P) around the surfaces of semi-circular cylinders. The value of C_P is used to measure pressure recovery at a particular surface location of the cylinder compared to the pressure value at the entrance (P_∞). Fig. 4 shows the variation of pressure coefficients (C_{p1} and C_{p2}) for both cylinders at different distance values between cylinders (Y_C) at extreme values of Re, Pr, and Ri. For Re = 1, Pr = 0.7 and Ri = 0, magnitudes of C_{p1} values are higher than values of C_{p2} at the curved surface of the cylinder at all values of Y_C, but reverse phenomena have been observed at the flat surface of the cylinder. This is because the curved surface of the upstream cylinder is facing the upcoming flow direction. For the upstream cylinder, the values of C_{p1} are found in accordance with the literature values [20]. The values of C_{p1} on curved surface are increased due to a change in value of Y_C from 1 to 4, but values of C_{p1} on flat surface are reported to be almost constant with an increase in values of Y_C. It shows the influence of the downstream cylinder presence and Y_C. In case of the downstream cylinder, initially, C_{p2} values are increased with increase in Y_C values from 1 to 3, then there is a cross-over between points A and B and a reverse trend is seen. The magnitudes of C_{p2} at the flat side of the cylinder are also increased with an increase in Y_C value. A similar variation of magnitudes of C_{p1} and C_{p2} values have been observed at curved surface and flat surface of cylinders for Re = 1, Pr = 50 and Ri = 2, with variation in Y_C values.

For Re = 50, Pr = 0.7 and Ri = 0, values of C_{p1} and C_{p2} are compared at the curved surface of the cylinder surface and have shown complex behavior at all values of Y_C. For similar Re, Pr and Ri values, magnitudes of C_{p1} at the flat surface are lower than C_{p2} at Y_C = 1 to 3 and higher than C_{p2} at Y_C = 4 to 6. The values of C_{p1} at curved surface are reported to decrease with an increase of Y_C in range of 1-3 only, reverse as observed at Re = 1. Conversely, the values of C_{p1} at flat surfaces are reported to be almost constant with an increase in values of Y_C. The variation of magnitudes of C_{p2} at the curved surface is reported to show complex behavior with a change in value of Y_C.

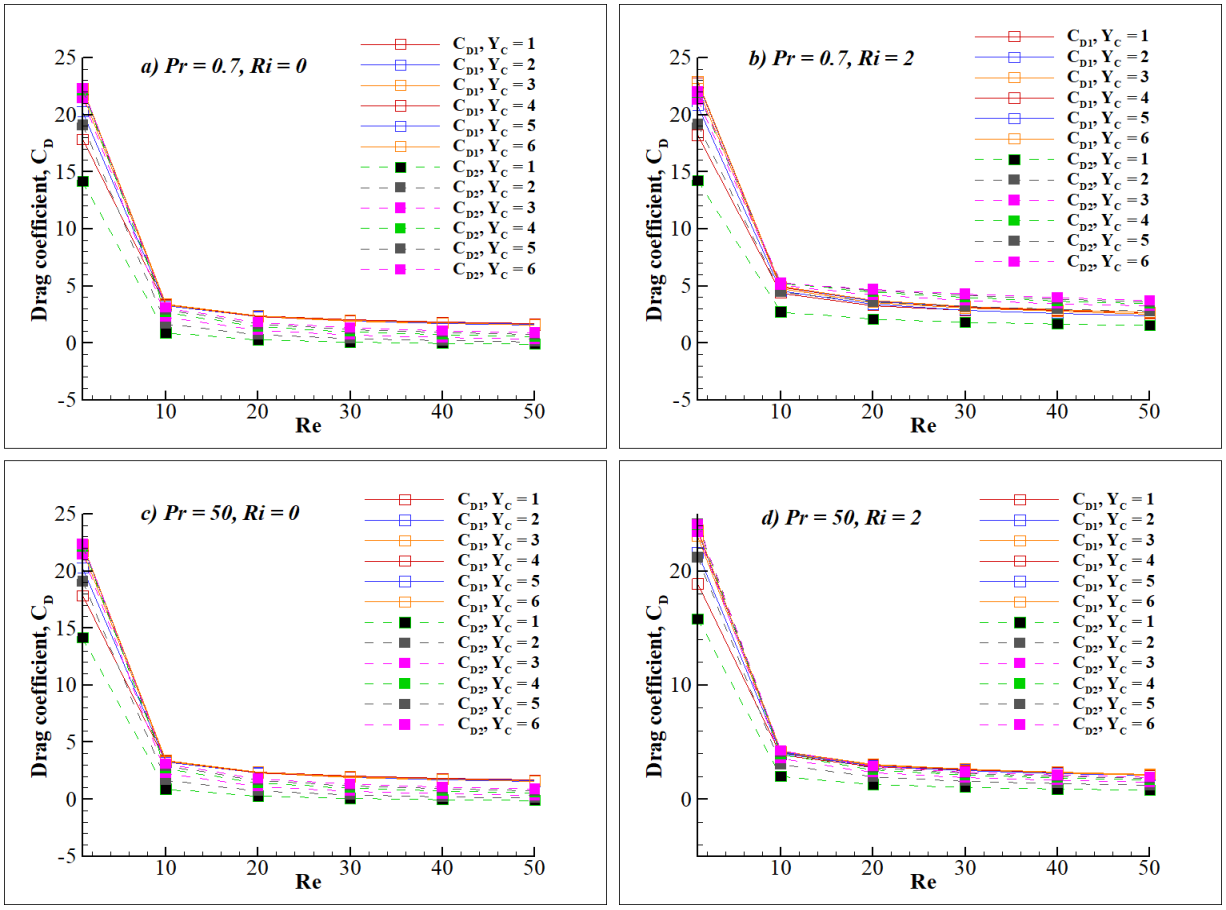

Fig. 5: Variation of drag coefficients with Reynolds numbers at different values of Pr, Ri and Y_C.

The magnitudes of C_{p2} values at the flat side of the cylinder are decreased with the increase of Y_C values. At Re = 50, Pr = 50, and Ri = 2, the values of C_{p1} at curved surface are increased with the increase of Y_C, in intervals of Y_C = 1-6. Otherwise, the variation of patterns of C_{p1} as well as C_{p2} with Y_C at Re = 50, Pr = 50, and Ri = 2 are found to be similar as reported at Re = 50, Pr = 0.7 and Ri = 0. For all cases, complex dependency of pressure coefficient on the governing parameters has been observed, and no clear trend has been found.

Drag coefficients

The drag coefficient is a measure of the total drag force on a cylinder due to fluid flow phenomena. It is helpful to determine the pressure drop across a bluff body and is used to evaluate the stability of the bluff body in the flow field. The estimated values of drag coefficients are used in the engineering/design calculations to develop engineering systems/equipment such as heat exchangers, underwater pipelines, power distribution lines (high tension lines), etc. The drag coefficients on both cylinders, as the functions of Re, Y_C, Pr and Ri, are given in Fig. 5. The thorough observations of Fig. 5 show that the individual values of C_{D1} and C_{D2} are decreased with an increase of Re for all values of other parameters. A similar trend of drag coefficients was also reported in our previous work on unconfined semi-circular cylinder [13]. Significant changes in drag values have been observed in the lower Re range (Re = 1-10). This may be due to the thick hydrodynamic boundary layer compared to its higher range of Re (as Re = 10-50). This happened due to the domination of viscous forces over inertia forces at lower Re, which is in line with the phenomenon reported in the literature [42,43].

Further, in Fig. 5, for Ri = 0 and Pr = 0.7 and 50, the value of C_{D1} is higher than C_{D2} for $1 \leq Y_C \leq 4$ and $Re \geq 10$. This trend is obvious because the upstream cylinder is directly facing the upcoming flow, whereas the second cylinder is facing the downstream flow from the first cylinder. The difference in C_{D1} and C_{D2} for a particular set

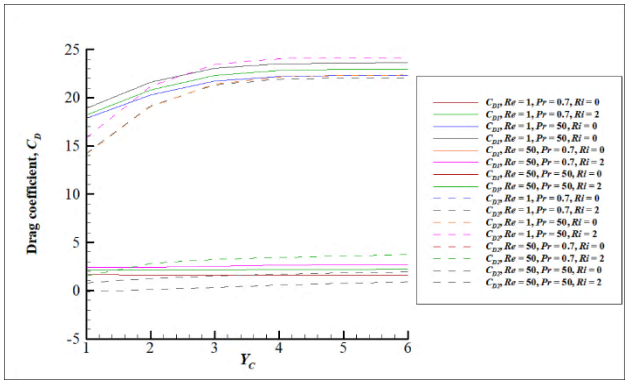

Fig. 6: Variation of Drag coefficients with values of Y_C at different values of Re, Pr and Ri.

of operating conditions is decreased as the Y_C value is increased. This trend is deviating at Y_C = 5, 6 and *Re* = 1. This phenomenon shows that the influence of upstream cylinder on the downstream cylinder is decreasing with the rising Y_C value. The C_{D1} value is found to increase with the value of Y_C at *Re* = 1-10, whereas for *Re* = 10-50, the value of C_{D1} has shown a negligible increase with an increase in value of Y_C. It concludes that the value of Y_C has negligible influence on C_{D1} and the upstream cylinder behaves like a single-cylinder at whole range of *Re*. The C_{D2} are seen to increase with an increase of Y_C and *Re* for its complete ranges ($1 \leq Y_C \leq 6$; $1 \leq Re \leq 50$). This trend shows that the presence of the upstream cylinder influences the downstream cylinder even at Y_C = 6 and all *Re* values. Further, For *Ri* = 2 and *Pr* = 0.7, C_{D1} value is found to be higher as compared to C_{D2}, only for operating sets of *Re* = 1, Y_C = 1-6; *Re* = 10, Y_C = 1-2; and *Re* = 20-50, Y_C = 1 only. For *Ri* = 2 and *Pr* = 50, the value of C_{D1} is found to be higher as compared to C_{D2} for all operating sets of *Re* and Y_C except *Re* = 1, Y_C = 3-6 and *Re* = 10, Y_C = 6. These values of C_{D1} and C_{D2} are also increased with an increase in Y_C value for all *Re* values. The effect on C_{D1} and C_{D2} is due to the combined and mixed influence of the governing parameters and flow geometry.

Fig. 6 shows a variation of the drag coefficients at both cylinders concerning the distance between cylinders at extreme values of other operating conditions *Re* = 1 and 50, *Pr* = 0.7 and 50, and *Ri* = 0 and 2. Drag coefficients at *Re* = 1 are found significantly higher as compared to values at *Re* = 50 at all other operating conditions. It is due to the domination of viscus forces at a low value of *Re*. At *Re* = 1, the values of C_{D1} and C_{D2} are increased with a rise in Y_C value for $1 \leq Y_C \leq 4$. Afterward, drag coefficient values remain unchanged in the range of $4 \leq Y_C \leq 6$. Hence, the presence of the upstream cylinder has negligible influence on the downstream cylinder for $4 \leq Y_C \leq 6$. Further, at *Re* = 50, the C_{D1} remains almost constant and the value of C_{D2} increases with an increase in Y_C value. Moreover, the C_{D1} value increases with a rise in *Ri* for all *Re*, *Pr* and Y_C values. The value of C_{D2} is increased as value of *Ri* increases for all values of *Re*, *Pr* and Y_C except at *Re* = 1, *Pr* = 0.7 and $3 \leq Y_C \leq 6$. At *Ri* = 0, the values of C_{D1} and C_{D2} are seen as constant, with the rising *Pr* value for all *Re* and Y_C values. Both drag coefficients at *Ri* = 2 are increased with *Pr* value at *Re* = 1 and decrease at *Re* = 50. Hence, the C_{D1} and C_{D2} values show the complex functional dependencies on the governing parameters considered in the present work.

Thermal characteristics

The thermal characteristics of the chosen flow configuration (Fig. 1) are presented as the isotherm profiles and the average Nusselt number for the ranges of the parameters considered here.

Isotherm profiles

Isotherm profiles depict the variation of temperature and temperature gradients in the flow field. In this view, the isotherm profiles around heated cylinders are shown in Fig. 7 for various sets of Y_C, *Re*, *Pr* and *Ri* values. The crowing of isotherms nearby a solid surface result in a thin thermal boundary layer and a higher heat transfer rate. The crowding of isotherms around both cylinders is observed at a higher value of either *Re* or *Pr* for every set of Y_C and *Ri*. Isotherms have negligible change with increase in *Ri* values at all sets of *Re*, *Pr* and Y_C except *Re* = 50 and *Pr* = 50. At *Re* = 50 and *Pr* = 50, isotherms show great impact of *Ri*. This may be due to the high Peclet number (*Re.Pr*), and shows higher convective heat transfer than the diffusive heat transfer. This heat transfer further increased in the presence of two nearby bluff bodies and the influence of buoyancy force at *Ri* = *2*. So, this phenomenon is more prominent at *Ri* = 2 than *Ri* = *0*.

In other words, the boundary layers of both cylinders are overlapped and showed significant interaction at the lower value of *Re*, *Pr* and Y_C. The thermal boundary layers of both cylinders are observed to be separated from each other at a higher value of *Re*, *Pr* and Y_C. This influence is seen more at *Re* = 50, *Pr* = 50. At *Re* = 50, *Pr* = 50 and Y_C

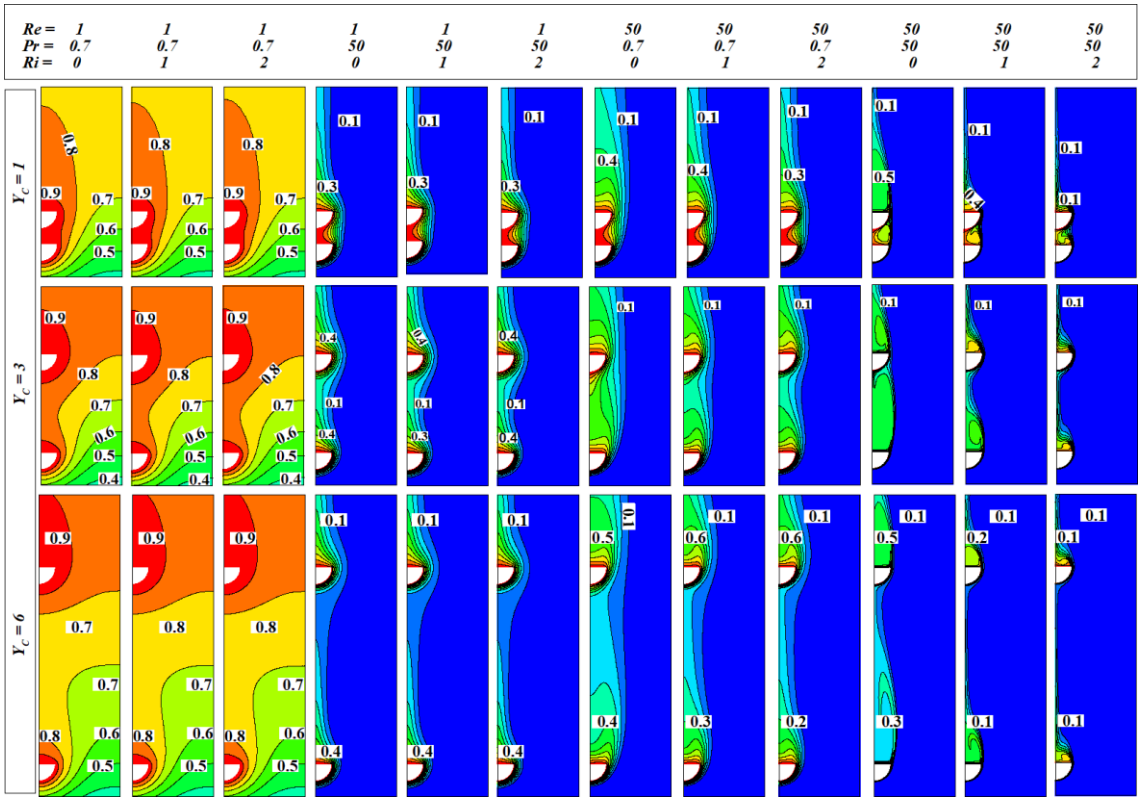

Fig. 7: Isotherm profiles at different values of Y_C, Re, Pr and Ri.

≥ 3, the impact of the upstream cylinder on the downstream cylinder is negligible due to the shortened boundary layer, and the presence of the upstream cylinder does not affect the flow and thermal field of the downstream cylinder. At Y_C = 6, a similar pattern has been seen for *Re* = 50 at all values of other parameters.

Average Nusselt Number (Nu_{avg})

The dimensionless heat transfer coefficient is presented in the form of the average Nusselt number (Nu_{avg}) for the current ranges of the parameters. The variation of values of Nu_{avg} for both semi-circular cylinders are represented in Fig. 8 at Y_C = 1, 3 and 6; *Pr* = 0.7 and 50; and *Ri* = 0, 1 and 2. The inspection of Fig. 8 shows that the values of Nu_{avg} are monotonically increasing with an increase in *Re* at every value of Y_C, *Pr* and *Ri*. Further, Nu_{avg} is increasing with an increase in *Pr* for all sets of Y_C, *Re* and *Ri*. The Nu_{avg} are found more in the case of the upstream cylinder (Nu_{avg1}) as compared to the downstream cylinder (Nu_{avg2}) at all operating conditions. This is because the upstream cylinder faces the upcoming flow at the initial temperature (low temperature), releases heat to the fluid due to a higher thermal gradient, and attains the increased fluid temperature. After the upstream cylinder, there is a downstream cylinder with the same temperature. The fluid approaches the downstream cylinder with a higher temperature than the inlet temperature. So, the downstream cylinder's thermal gradient is reduced, leading to a lower heat transfer rate and lower value of Nu_{avg2}.

Further, the difference in the values of Nu_{avg1} *and* Nu_{avg2} is decreased with an increase in Y_C because of the decreasing influence of the upcoming cylinder and the larger convection region among the two cylinders by increasing the value of Y_C. This larger convection region limits the higher temperature zone near the upstream cylinder, and the approaching fluid to the downstream cylinder gets cool. So, the heat transfer from the downstream cylinder increases at higher Y_C. Furthermore, the values of Nu_{avg} at *Pr* = 0.7 are increased with *Ri*, but Nu_{avg} at *Pr* = 50 is varied in a mixed/complex pattern with a variation of *Ri* at all Y_C and *Re*.

Furthermore, Fig. 9 presents the average Nusselt numbers (Nu_{avg1} and Nu_{avg2}) for both cylinders with variation in distance between cylinders (Y_C) for various sets of *Re*, *Pr* and *Ri*. The values of Nu_{avg1} and Nu_{avg2} at *Re* = 50

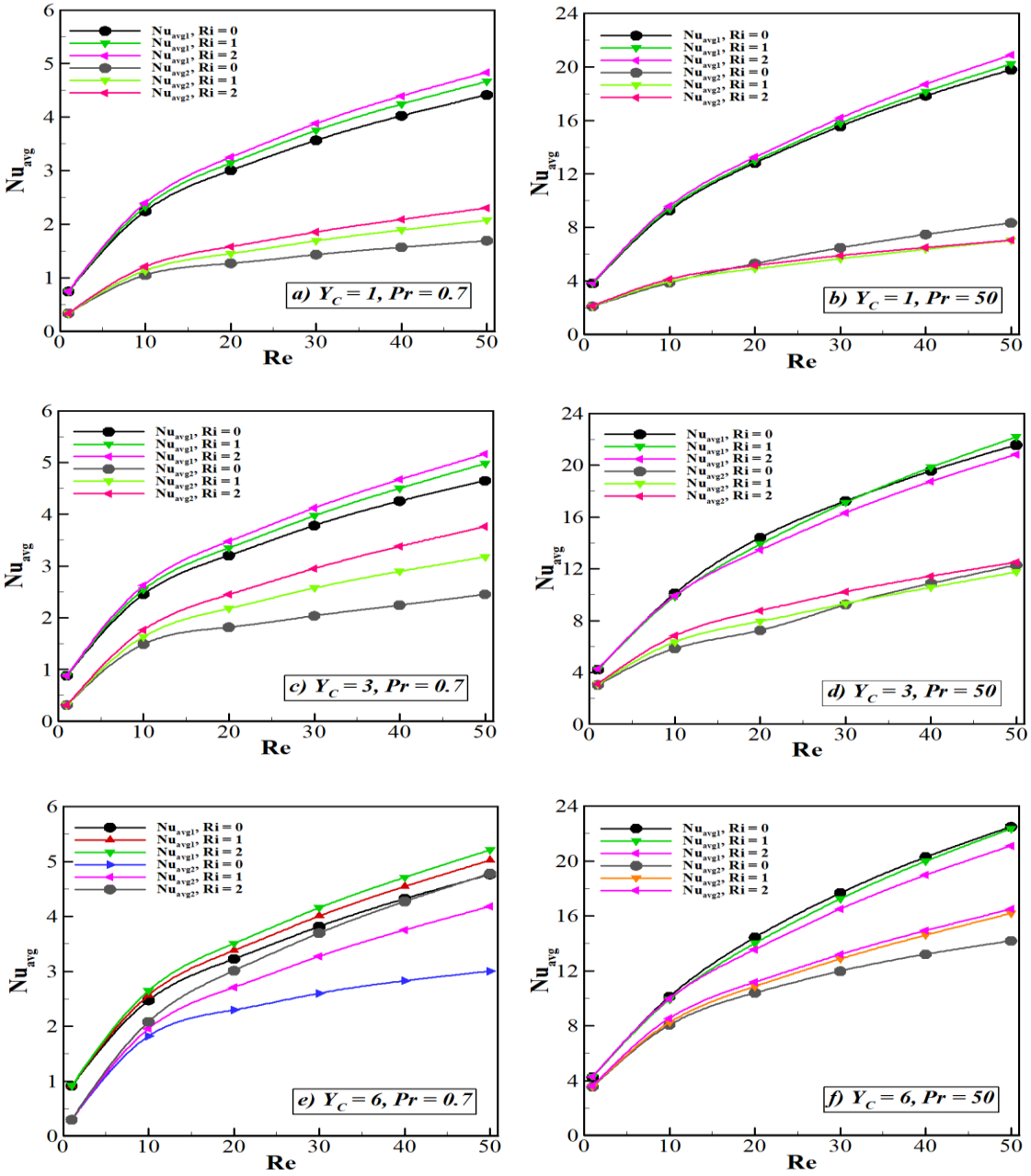

Fig. 8: Variation of average Nusselt number with Reynolds numbers at different values of Y_C, Pr and Ri.

are higher and varied by a change in values of *Ri*, as compared to their corresponding values at *Re* = 1. with no change with *Ri*. The value of Nu_{avg1} at *Pr* = 0.7 increases little due to a rise in Y_C value and, afterwards, remains almost constant at both values of *Re* = 1 and 50. At a higher value of *Pr* (= 50), a similar trend of Nu_{avg1} has been observed with an increase in Y_C value. Further, Nu_{avg2} values at *Pr* = 0.7 are reported to be constant at *Re* = 1, whereas it increases at *Re* = 50 with Y_C. At a higher value of *Pr* (= 50), Nu_{avg2} has been increased with an increase in Y_C value at both *Re* values (= 1 and 50). Therefore, the effect of cylinder spacing on heat transfer coefficient is more dominant at a higher *Re* value.

CONCLUSIONS

This study presented flow and thermal characteristics for semi-circular cylinders in a tandem arrangement under vertical confinement (β = 0.2) for Newtonian fluids.

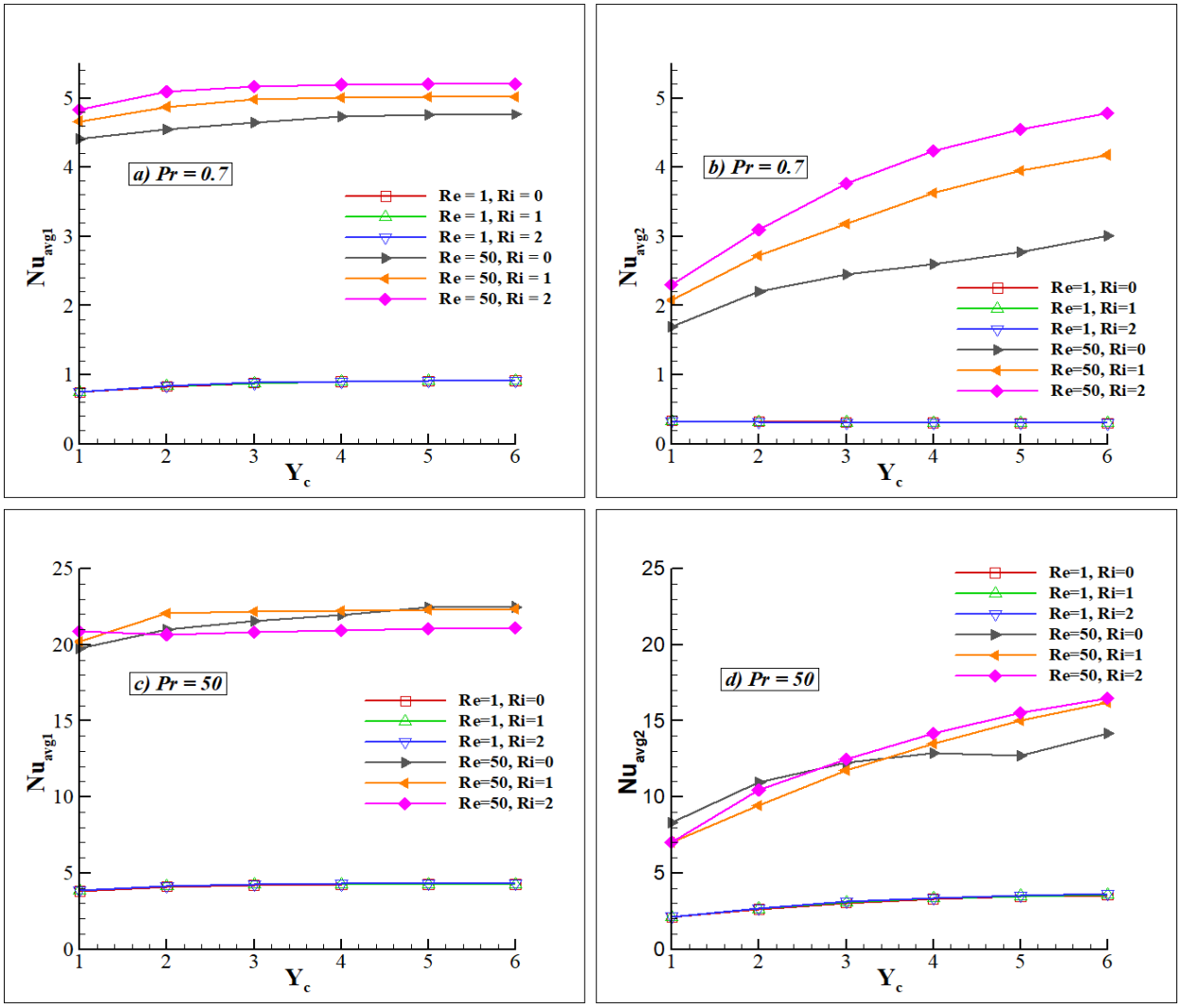

Fig. 9: Variation of average Nusselt number with the distance between cylinders at different values of Pr, Re, and Ri.

The interaction of upstream and downstream cylinders showed complex dependency with all the governing parameters. The spacing between cylinders (Y_C) significantly affected the streamlines, pressure coefficient, drag coefficient, isotherms profile and average Nusselt number. Specifically, the value of the drag coefficient for an upstream cylinder depends on Y_C for $1 \leq Re \leq 10$. But in the range of $10 \leq Re \leq 50$, the drag coefficient for the upstream cylinder has shown no change with respect to the value of Y_C except for the case of $Pr = 0.7$ and $Ri = 2$. Moreover, the value of the drag coefficient for the downstream cylinder has increased with the increase in the value of Y_C, irrespective of its Re value. A substantial change in drag coefficients at $Re = 1$ has been seen for $Y_C \leq 4$. Further, higher heat transfer from cylinders has been observed at higher cylinder spacing. The average Nusselt number of both cylinders has increased with an increase in the value of Y_C except for the case of $Re = 1$ and $Pr = 0.7$ for a downstream cylinder. Moreover, the rise in Re and Pr enhanced the values of Nu_{avg} and C_D, whereas Ri showed complex dependency. The highest Pr value used in the study has been 50, considering its practical importance even in the use of high viscous or high molecular weight fluids (e.g. Polymer melts, sucrose solutions, light organic oils, etc.) in chemical, food, petroleum, and oil industries. The present work will be helpful for the further development of more efficient and effective heat transfer equipment. The multivariable optimization of flow and heat transfer parameters may be considered for further extension of this work. A multivariate method for the flow

and heat transfer analysis can also be proposed for future work [44,45].

Nomenclature

Drag coefficient at the surface of semi-circular cylinder (dimensionless)	C_D
Drag coefficient at the surface of upstream semi-circular cylinder (dimensionless)	C_{D1}
Drag coefficient at the surface of downstream semi-circular cylinder (dimensionless)	C_{D2}
Specific heat capacity of the fluid (J/kg K)	c_p
Pressure coefficient at the surface of upstream semi-circular cylinder (dimensionless)	C_{P1}
Pressure coefficient at surface of downstream semi-circular cylinder (dimensionless)	C_{P2}
Diameter of the cylinder (m)	D
Total number of the elements in computational domain (dimensionless)	G_N
Drag force per unit length of the cylinder (N/m)	F_D
Width of the rectangular channel (m)	L
Distance of inlet domain (m)	M
Dimensionless distance of inlet domain [=M/D] (dimensionless)	m
Distance of outlet domain (m)	N
Dimensionless distance of outlet domain [=N/D] (dimensionless)	n
Number of grid points on the surface of the cylinder (dimensionless)	n_p
Local Nusselt number (dimensionless)	Nu
Average Nusselt number of cylinder surface (dimensionless)	Nu_{avg}
Average Nusselt number of upstream cylinder surface (dimensionless)	Nu_{avg1}
Average Nusselt number of downstream cylinder surface (dimensionless)	Nu_{avg2}
Fluid pressure (Pa)	P
Static pressure at cylinder surface (Pa)	P_S
Fluid pressure at channel inlet (Pa)	P_∞
Prandtl number [= $c_p\mu/k$] (dimensionless)	***Pr***
Reynolds number [= $DV_\infty\rho/\mu$] (dimensionless)	Re
Richardson number [= $g\,\beta_V(T - T_\infty)D/V_\infty^2$] (dimensionless)	Ri
Fluid absolute temperature (K)	T
Fluid temperature at the inlet section (K)	T_∞
Wall temperature of cylinder (K)	T_w
Fluid velocity in *X*-direction (m/s)	U
Fluid velocity in *Y*-direction (m/s)	V
Average velocity at channel inlet (m/s)	V_∞
Cartesian co-ordinates (m)	X, Y
Distance between centres of the cylinders (m)	Y_C

Greek Letters

Blockage ratio of confinement [= D/L] (dimensionless)	β
Coefficient of thermal volumetric expansion of fluid (K^{-1})	β_V
Grid spacing at the surface of the cylinder (dimensionless)	δ
Fluid density (kg/m^3)	ρ
Fluid density at temperature of T_∞ (kg/m^3)	ρ_∞
Fluid temperature (dimensionless)	θ

Subscripts

Film temperature	f

Received : Aug.26,2022 ; Accepted : Oct.31, 2022

REFERENCES

[1] Chatterjee D., Mixed convection Heat Transfer from Tandem Square Cylinders in A Vertical Channel at low Reynolds Numbers, *Numer. Heat Tr. A-Appl.*, **58:** 740–755 (2010).

[2] Gode A., Sahu A.K., Chhabra R.P., Two-Dimensional Steady Flow Over a Semi-Circular Cylinder: Drag Coefficient and Nusselt Number, *Int. J. Adv. Eng. Sci. Appl. Math.*, **3(1-4)**: 44-59 (2011).

[3] Ali R., Singh A., Numerical Study of Fluid Dynamics and Heat Transfer Characteristics for the Flow Past a Heated Square Cylinder, *Jordan J. Mech. Ind.*, **15**: 357-376 (2021).

[4] Pawar A.P., Sarkar S., Saha S.K., Forced Convective Flow and Heat Transfer Past an Unconfined Blunt Headed Cylinder at Different Angles of Incidence, *Appl. Math. Modell.*, **82**: 888-915 (2020).

[5] Laidoudi H., Bouzit M., Effect of Thermal Buoyancy on Flow Pattern from a Pair of Side-by-Side Confined Triangular Cylinders, *Bangladesh J. Sci. Ind. Res.*, **55(1)**: 9-14 (2020).

[6] Meibodi M.E., Anvari A., Javaherdeh K., The Non-Dimensional Analysis of Heat transfer and Fluid Flow in Wavy Mini Channel Heat Exchangers, *Iran. J. Chem. Chem. Engg.*, **41(4):** 1370-1380 (2022).

[7] Habibi M.R., Amini M., Arefmanesh A., Ghasemikafrudi E., Effects of Viscosity Variations on Buoyancy-Driven Flow from a Horizontal Circular Cylinder Immersed in Al_2O_3-Water Nanofluid, *Iran. J. Chem. Chem. Engg. (IJCCE)*, **38(1)**: 213-232 (2019).

[8] Nada S.A., Mowad M., Free convection from A Vertical and Inclined Semicircular Cylinder at Different Orientations, *Alexandria Eng. J.*, **42(3)**: 273-282 (2003).

[9] Nada S.A., El-Batsh H., Moawed M., Heat Transfer and Fluid Flow Around Semi-Circular Tube in Cross Flow at Different Orientations, *Heat Mass Transfer*, **43**: 1157-1169 (2007).

[10] Chandra A., Chhabra R.P., Momentum and Heat Transfer Characteristics of a Semi-Circular Cylinder Immersed in Power-Law Fluids in the Steady Flow Regime, *Int. J. Heat Mass Transf.*, **54**: 2734-2750 (2011).

[11] Chandra A., Chhabra R.P., Flow Over and Forced Convection Heat Transfer in Newtonian Fluids from a Semi-Circular Cylinder, *Int. J. Heat Mass Transf.*, **54**: 225-241 (2011).

[12] Bhinder A.P.S., Sarkar S., Dalal A., Flow Over and Forced Convection Heat Transfer Around a Semi-Circular Cylinder at Incidence, *Int. J. Heat Mass Transf.*, **55**: 5171–5184 (2012).

[13] Chandra A., Chhabra R.P., Mixed Convection from a Heated Semi-Circular Cylinder to Power-Law Fluids in the Steady Flow Regime, *Int. J. Heat Mass Transf.*, **55**: 214–234 (2012).

[14] Chung H.S., Lee G.H., Nine M.J., Bae K., Jeong H.M., Study on the Thermal and Flow Characteristics on the Periodically Arranged Semi-Circular Ribs in a Rectangular Channel, *Exp. Heat Transf.*, **27**: 56–71 (2014).

[15] Sukesan M.K., Dhiman A.K., Laminar Mixed Convection in a Channel with a Built-in Semi-Circular Cylinder under the Effect of Cross-Buoyancy, *Int. Commun. Heat Mass Transf.*, **58**: 25–32 (2014).

[16] Kumar A., Dhiman A., Laminar Flow and Heat transfer Phenomena Across a Confined Semicircular Bluff Body at Low Reynolds Numbers, *Heat Transf. Eng.*, **36(18)**: 1540-1551 (2015).

[17] Kumar A., Dhiman A., Baranyi L., CFD Analysis of Power-Law Fluid Flow and Heat Transfer Around a Confined Semi-Circular Cylinder, *Int. J. Heat Mass Transf.*, **82**: 159-169 (2015).

[18] Parthasarathy N., Dhiman A., Sarkar S., Flow and Heat Transfer over a Row of Multiple Semi-Circular Cylinders: Selection of Optimum Number of Cylinders and Effects of Gap Ratios, *Eur. Phys. J. Plus.*, **132(532)**: 1-23 (2017).

[19] Sisodia S.S., Sarkar S., Saha S.K., Fluid Flow and Mixed Convective Heat Transfer Around a Semi-Circular Cylinder at Incidence with a Tandem Downstream Square Cylinder in Cross Flow, *Int. J. Therm. Sci.*, **121**: 13-29 (2017).

[20] Gupta R.K., Chandra A., Gupta R.K., Buoyancy-Driven Convective Heat Transfer from a Semi-Circular Cylinder for Various Confinements, *Sadhana*, **43(182)**: 1-18 (2018).

[21] Sahu M.K., Pandey K.M., Chatterjee S., Thermo-Hydraulic Performance of Rectangular Channel Roughened with Combined Semi-Circular and Triangular Ribs, *Heat Mass Transf.*, **55:** 2889–2900 (2019).

[22] Khoshvaght-Aliabadi M., Arani-Lahtari Z., Forced Convection in Twisted Minichannel (TMC) With Different Cross Section Shapes: A Numerical Study, *Appl. Therm. Eng.*, **93**: 101-112 (2016).

[23] Khoshvaght-Aliabadi M., Deldar S., Hassani S.M., Effects of Pin-Fins Geometry and Nanofluid on the Performance of a Pin-Fin Miniature Heat Sink (PFMHS), *Int. J. Mech. Sci.*, **148**: 442-458 (2018).

[24] Srinivas A.T., Bharti R.P., Chhabra R.P., Mixed Convection Heat Transfer from a Cylinder in Power-Law Fluids: Effect of Aiding Buoyancy, *Ind. Eng. Chem. Res.*, **48**:9735-9754 (2009).

[25] Chatterjee D., Mondal B., Forced Convection Heat Transfer from an Equilateral Triangular Cylinder at Low Reynolds Numbers, *Heat Mass Transf.*, **48:** 1575-1587 (2012).

[26] Chandra A., Chhabra R.P., Momentum and Heat Transfer from a Semi-Circular Cylinder to Power-Law Fluids in the Vortex Shedding Regime, *Numer. Heat Tr. A-Appl.*, **63**: 489-510 (2013).

[27] Rao P.K., Sasmal C., Sahu A.K., Chhabra R.P., Eswaran V., Effect of Power-Law Fluid Behavior on Momentum and Heat Transfer Characteristics of an Inclined square Cylinder in Steady Flow Regime, *Int. J. Heat Mass Transf.*, **54:** 2854-2867 (2011).

[28] Nirmalkar N., Chhabra R.P., Poole R.J., Laminar Forced Convection Heat Transfer from a Heated Square Cylinder in a Bingham Plastic Fluid, *Int. J. Heat Mass Transf.*, **56**: 625-639 (2013).

[29] Hatton A.P., James D.D., Swire H.W., Combined Forced and Natural Convection with Low-Speed Air Flow Over Horizontal Cylinders, *J. Fluid Mech*., **42**(1): 17-31 (1970).

[30] Lacroix M., Carrier R., Mixed Convection Heat Transfer from Vertically Separated Horizontal Cylinders within Confining Walls, *Numer. Heat Transf. Part A Appl*., **27(4)**: 487-498 (1995).

[31] Gowda Y.T.K., Narayana P.A.A., Seetharamu K.N., Mixed Convection Heat Transfer Past in-Line Cylinders in a Vertical Duct, *Numer. Heat Transf., Part A Appl*., **31(5)**: 551-562 (1997).

[32] Salcedo E., Trevino C., Cajas J.C., Martinez-Suastegui L., Unsteady Mixed Convection from Two Isothermal Semicircular Cylinders in Tandem Arrangement, *Heat Exchangers: Design, Experiment And Simulation, Intechopen, London*, 221-241, (2017).

[33] Kaur R., Sharma S., Chandra A., Air Flow Around and Through a Permeable Semi-Circular Cylinder, *Chem. Eng. Technol*., **45(3)**: 449–455 (2022).

[34] Kaur R., Sharma S., Chandra A., Convective Heat Transfer from a Porous Semi-Circular Obstacle Attached to a Channel Wall, *Chem. Eng. Technol*., **45(6)**: 1075–1086 (2022).

[35] Kaur R., Chandra A., Sharma S., Momentum Transfer Across a Semi-Circular Porous Cylinder Attached to a Channel Wall, *Meccanica*, **56**: 2219-2241 (2021).

[36] Ismael M.A., Mansour M.A., Chamkha A.J., Rashad A.M., Mixed Convection in a Nano Fluid Filled-Cavity with Partial Slip Subjected to Constant Heat Flux and Inclined Magnetic Field, Mixed Convection in a Nano Fluid Filled-Cavity with Partial Slip Subjected to Constant Heat Flux and Inclined Magnetic Field, *J. Magn. Magn. Mater*., **416**: 25-36 (2016).

[37] Rashad A.M., Ismael M.A., Chamkha A.J., Mansour M.A., MHD Mixed Convection of Localized Heat Source/Sink in a Nanofluid-Filled Lid-Driven Square Cavity with Partial Slip, *J. Taiwan Inst. Chem. Eng*., **68**: 173-186 (2016).

[38]Chamkha A. J., Rashad A. M., Mansour M. A., Armaghani T., Ghalambaz M., Effects of Heat Sink and Source and Entropy Generation on MHD Mixed Convection of a Cu-Water Nanofluid in a Lid-Driven Square Porous Enclosure with Partial Slip, *Phys. Fluids*, **29(5)**: 1-23 (2017).

[39] Rashad A.M., Sivasankaran S., Mansour M.A., Bhuvaneswari M., Magneto-convection of Nanofluids in a Lid-Driven Trapezoidal Cavity with Internal Heat Generation and Discrete Heating, *Numer. Heat Transf. A*, **71(12)**: 1223-1234 (2017).

[40] Jafari A., Shahmohammadi A., Mousavi S.M., CFD Investigation of Gravitational Sedimentation Effect on Heat Transfer of a Nano-Ferrofluid, *Iran. J. Chem. Chem. Eng. (IJCCE)*, **34(1)**: 87-96 (2015).

[41] Farouk B., Guceri S.I., Natural and Mixed Convection Heat Transfer Around a Horizontal Cylinder Within Confining Walls, *Numer. Heat Transf*., **5**: 329-341 (1982).

[42] Zdravkovich M. M., "Flow Around Circular Cylinders Vol.1: Fundamentals", Oxford University Press, New York, (1997).

[43] Zdravkovich M. M., "Flow Around Circular Cylinders Vol.2: Applications", Oxford University Press, New York, (2003).

[44] Galliano S., Bella F., Piana G., Giaconaa G., Viscardi G., Gerbaldi C., Grätzel M., Barolo C., Finely tuning Electrolytes and Photoanodes in Aqueous Solar Cells by Experimental Design, *Sol. Energy*, **163**: 251-255 (2018).

[45] Xu D., Shen W., Sun S., Chen Y., Lu Z., Meng X., Wang C., Guo L., Liu C., Huang Q., Experimental Design of 1-dodecanol@Methylated Melamine-Formaldehyde Microencapsulated Composite Phase Change Material and the Application in Energy Storage Field, *J. Energy Storage*, **55:** Part A: 1-12 (2022).